

Shape of the ^8B alpha and neutrino spectra

C.E. Ortiz¹, A. García^{1,2}, R. A. Waltz¹, M. Bhattacharya^{1,a} and A. K. Komives¹

¹ University of Notre Dame, Notre Dame, Indiana 46556

² Lawrence Berkeley National Lab, Berkeley, California 94720

The β -delayed α spectrum from the decay of ^8B has been measured with a setup that minimized systematic uncertainties that affected previous measurements. Consequently the deduced neutrino spectrum presents much smaller uncertainties than the previous recommendation [1]. The ^8B ν spectrum is found to be harder than previously recommended with about (10-20)% more neutrinos at energies between 12-14 MeV. The efficiencies of the ^{37}Cl , ^{71}Ga , ^{40}Ar , and SuperKamioka detectors are respectively, 3.6%, 1.4%, 5.7% and 1.8% larger than previously thought.

The solar neutrino detectors SuperKamiokande, SNO, and ICARUS, are sensitive primarily to neutrinos from the decay: $^8\text{B} \rightarrow ^8\text{Be} + e^+ + \nu_e$. The expected differences between the shape of this neutrino spectrum in the laboratory and in the sun are small [2]. Hence any observed difference between the shape of this spectrum as measured in the laboratory compared to that measured by solar neutrino detectors would imply non-standard physics. For example, when the spectrum from SuperKamiokande is compared to the expected spectrum based on laboratory measurements [1], one observes not just an overall reduction in the number of neutrinos but also a distortion of the spectrum, *i.e.*, the reduction is not as severe for the high-energy end of the spectrum (between 12 to 14 MeV) as it is for lower energies. This has motivated several authors to try to find possible explanations ranging from the physical (hep neutrinos [3–5], electron capture [6]) to the systematic (energy calibration uncertainties in SuperKamiokande [7]).

The β^+ decay of ^8B ($J^\pi = 2^+$) is dominated by a transition to a state at $E_x \approx 3$ MeV ($J^\pi = 2^+$) with a width of ≈ 1.5 MeV. Because this is a broad state, its interference with other 2^+ states at higher energies affects the spectrum, and the final state distribution has to be determined experimentally. There have been 4 previous measurements of the α spectrum: one by Farmer and Class (FC) [8], one by DeBraekeleer and Wright (DBW) (not published), and two by Wilkinson and Alburger, one with a thick catcher foil (WA1) and one with a thin catcher foil (WA2) [9]. Because statistics are highest at the peak of the spectrum, Bahcall *et al.* [1] compared the different spectra by varying the energy calibration offset. They showed that in order to get the best agreement with the β^+ spectrum of Napolitano and Freedman [10] the α spectra had to be shifted as follows: FC by ≈ -85 keV; DBW by $\approx +75$ keV; WA2 by $\approx +65$ keV; and WA1 by $\approx +25$ keV. The high statistics measurement of Wilkinson and Alburger was motivated to search for Second Class Currents [9] by comparing the delayed- α spectra from ^8Li and ^8B decay. Consequently their measurement

was optimized towards studying the *relative* differences between the two spectra and not their *absolute* shape. Given the importance of an accurate knowledge of the shape of the ^8B neutrino spectrum, this state of affairs is unsatisfactory.

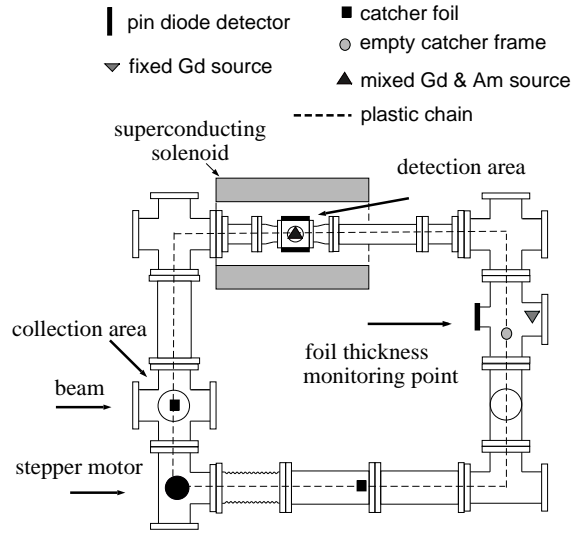


FIG. 1. Overhead view of the experimental setup.

A common problem encountered by the previous measurements of the delayed- α spectrum is the energy summing of the α 's with the preceding β^+ 's, resulting in a distortion of the spectrum. In order to minimize this effect previous authors used small-solid-angle detectors. In addition, measuring the spectrum in singles, as was done by previous authors, entails subtracting low-energy β^+ backgrounds and possible events originating from ^8B 's implanted in the frame of the catcher foil, correcting for shifts in the α energy due to the recoiling nucleus and α -energy losses at different depths in the catcher foil, all of which can introduce systematic distortions if not properly accounted for. Finally, all previous experiments had to be interrupted to perform detector energy calibrations.

In this paper the results from an α spectrum measurement, that overcame all of the difficulties discussed above, are presented.

Figure 1 shows a top view of the setup. Catcher foils ($20 \mu\text{g}/\text{cm}^2$ of ^{12}C) mounted on Al frames attached to

^aPresent address: Nuclear Physics Laboratory, University of Washington, Seattle, Washington 98195

a chain were transported through three stations by a computer-controlled stepper motor. At the first station a 5 MeV ^3He beam (typically of $\sim 0.25 \mu\text{A}$) impinged upon a target of 600 to 700 $\mu\text{g}/\text{cm}^2$ of 95% enriched ^6LiF evaporated onto a 10 $\mu\text{g}/\text{cm}^2$ Carbon foil. The beam energy was chosen to optimize the production at the target. Because the ^6LiF targets lasted only for a few hours of bombardment, several targets were mounted in a vertical-motion ladder, which allowed for quick replacement without having to break the vacuum. The radioactivity was collimated to make a 0.79 cm diameter circular spot on the catcher foils, while the hole in the Al frames for the catcher foils was 1.27 cm in diameter. The second station had two Hamamatsu Si PIN detectors with 256 mm^2 of effective area (after masking their edges) located 3.24 ± 0.16 cm from either side of the catcher foil. The counting chamber was placed inside the bore of a super-conducting solenoid which produced a 3.5-Tesla magnetic field perpendicular to the line joining the centers of the detectors. The magnetic field channeled the β 's away from the detectors. The third station was dedicated to monitor the catcher foil thickness by measuring the energy loss of ^{148}Gd α particles passing through the catcher foils. The catcher foil thicknesses were monitored throughout the data taking. During the course of the run the catcher foils grew thicker due to a combination of sputtering from the target and carbon build up on the beam spot due to imperfect vacuum, and were replaced when their thickness exceeded 30 $\mu\text{g}/\text{cm}^2$.

The data was taken by repeating cycles which consisted of four stages. In the first stage while radioactivity was being collected on the first catcher foil, both of the detectors at the counting station faced mixed ^{148}Gd ($E_\alpha \approx 3183$ keV) and ^{241}Am ($E_\alpha \approx 5443, 5486$ and 5499 , keV) thin α sources. At the end of the collection the chain and sprocket system (see Fig. 1) was rotated to the next position. The distance of ≈ 0.9 m from the loading to the counting station was covered in ≈ 0.9 s, so the radioactivity having a half life of less than a second could be counted efficiently. In the second stage the first catcher foil would be counted by the detectors at the counting station while the second one was being loaded. In the third stage the thickness of the first catcher foil was monitored at the thickness-monitoring station, while the second catcher foil was being counted at the counting station and an empty catcher-foil frame was at the collection area. The purpose of the empty frame was to monitor the radioactivity implanted in the aluminum frame. In the fourth and final stage the thickness of the second catcher foil was monitored while the empty catcher foil frame was at the detection area. The chain would then be rotated in the reverse direction until the system was back to the original position. Each collection-counting stage took ≈ 2.5 seconds. The incident beam was interrupted by a Faraday cup, located ~ 5 meters upstream of the system, every time the chain moved, to avoid depositing radioactivity in places other than the center of

the catcher foils.

The primary advantages of the experimental setup in light of the discussion above are:

1. As the detectors were placed in a 3.5-Tesla magnetic field, the positrons from the decay of ^8B could not reach the detectors while the delayed α 's suffered little deflection. This allowed the detection of $\alpha - \alpha$ coincidences without $\beta - \alpha$ contamination. This is a powerful tool to reject backgrounds and avoid counting α 's coming from radioactivity implanted in the Al frame. The coincidence summed spectra are also free of any recoil-broadening.
2. Energy calibrations of the detectors were performed during each cycle, without having to break the vacuum or un-bias the detectors to introduce calibration sources.
3. The foils thicknesses were monitored throughout the course of the experiment.

The signals were shaped using ORTEC 142A pre-amplifiers and ORTEC 572 amplifiers and digitized using an ORTEC 413A ADC. The trigger was defined as a hit in any one of the three detectors.

The recorded pulse heights were corrected for energy losses in the catcher foil and detector dead layers on an event-by-event basis. The largest corrections (at $E_\alpha = 0.5$ MeV) were ≈ 25 keV and ≈ 15 keV for energy losses in the catcher foil and detector dead layer respectively. The detectors dead layer was measured before and after the data taking by mounting the detectors on a rotating jig which allowed a measurement of the energy deposited by a ^{148}Gd α in the detector as a function of the angle between the normal to the source and the normal to the detector. The dead layers were assumed to be 100% Si and were found to be $9 \pm 2 \mu\text{g}/\text{cm}^2$ for both detectors. The α 's summed energy was also corrected for the effect of the recoiling ^8Be nucleus. The largest correction for this effect (at $E_{\alpha 1} + E_{\alpha 2} \approx 1.0$ MeV) was ≈ 8 keV. A Monte Carlo simulation was used to determine the average amount of energy each α would lose in the catcher foil and in the detector dead layers as well as the average velocity of the recoiling ^8Be nucleus as a function of the α 's energy.

One disadvantage of the experimental setup is the fact that the energy dependence of the α efficiency is magnified by the presence of the magnetic field. Figure 2 shows the average efficiency for detecting a pair of α particles as a function of the ^8Be excitation energy. The efficiency was calculated using a Monte Carlo code that took into account the effect of the magnetic field, the charge distributions of the α particles coming out of the Carbon foil, and the source size and position. The source size was determined by the collimators and confirmed by visual inspection of the catcher foils. The source position was monitored and found to be extremely stable during data taking. The ratio of coincidences to singles events

turned out to be a powerful tool in constraining systematic uncertainties. Using both sources of information the source position was constrained to ± 0.16 cm in all three spatial directions, and the diameter of the source spot to 0.79 ± 0.16 cm.

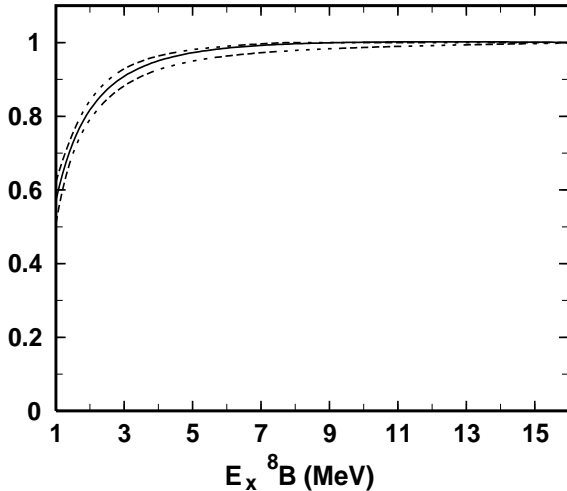


FIG. 2. Average efficiency (solid) and systematic uncertainties (dashed) for detecting a pair of α particles vs. excitation energy in ${}^8\text{Be}$. The upper dashed line represents the uncertainty in the efficiency due to the equilibrium thickness and the source’s diameter. The lower dashed line includes these uncertainties as well as those due to the source’s position (misalignment can only reduce the efficiency).

The *equilibrium* charge state distribution of α particles for a given energy was interpolated from the measured values quoted in Ref. [11]. The minimum thickness needed to reach equilibrium, x_{\min} , was estimated to be $\approx 5 \mu\text{g}/\text{cm}^2$. To account for possible uncertainties in this estimate of the charge state distribution, calculations were performed assuming $x_{\min} = 1, 5,$ and $10 \mu\text{g}/\text{cm}^2$; but this contribution to the uncertainty in the efficiency was found to be negligible. For all cases the charge distribution was assumed to follow a straight line between the equilibrium point, x_{\min} , and the edge of the foil, from where an α is emitted in the $q = +2$ state.

The data was fit under 8 different conditions. Under condition A each detector’s dead layer was assumed to be $9 \mu\text{g}/\text{cm}^2$ and each catcher foil was corrected for changes in thickness over time. Under condition B each detector’s dead layer was assumed to be $7 \mu\text{g}/\text{cm}^2$ and each catcher foil was assumed to be a constant $20 \mu\text{g}/\text{cm}^2$. Under condition C each detector’s dead layer was assumed to be $11 \mu\text{g}/\text{cm}^2$ and each catcher foil was assumed to be a constant $30 \mu\text{g}/\text{cm}^2$. Condition B underestimates the amount of energy lost in the dead layers and catcher foil, while condition C overestimates this quantity. Condition D was the same as A except that no line-shape correction was made. Three additional conditions, $E_x, E_y,$ and $E_z,$ were the same as A except that efficiency used was for a source displaced by 0.16 cm in the $x, y,$ and z spatial directions respectively. Condition E_d assumed an efficiency

for a source diameter 0.16 cm larger than expected. The statistical errors to the α spectrum were calculated as the square root of the number of raw counts divided by the relative efficiency. The systematic errors to the α spectrum were calculated by adding in quadrature the differences between the R-matrix fit under condition A to those under the 7 other conditions and condition A offset by 8.5 keV (the error in the calibration). A table with the results can be down-loaded [12].

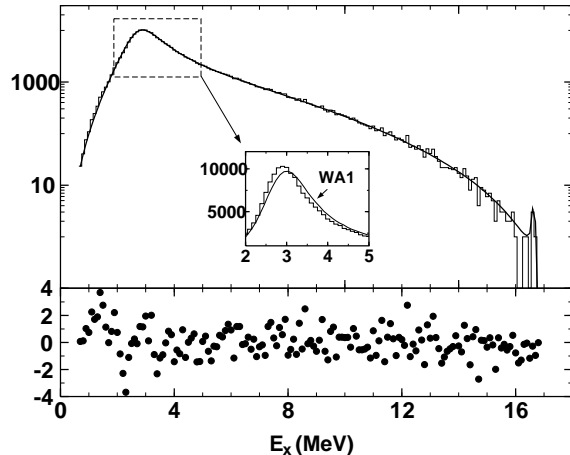


FIG. 3. Top panel: α spectrum and R-matrix fit. The insert compares this spectrum (stair step) to the WA1 spectrum (solid) normalized to have the same number of counts as this α spectrum. Bottom panel: residuals.

Figure 3 shows an R-matrix fit to our total α spectrum, which was performed following the prescriptions of Refs. [13,14] and limiting the fits to contain 4 resonances and not including an 8-MeV intruder state. The data is well described with $\chi^2/\nu \approx 1.1$ with $\nu \sim 160$, while the fits to the WA1 and WA2 spectra yield $\chi^2/\nu \approx 1.9$ and 2.2 , respectively, assuming only statistical errors. The inset shows a comparison between these data (histogram) and the WA1 spectrum (continuous line). The present spectrum peaks at a lower excitation energy.

The intensity of the second forbidden transition to the 0^+ ground state was estimated using the known Γ_γ widths [15] of the decays from the two states at $E_x \approx 16$ MeV and the Conserved Vector Current hypothesis to extract the matrix element. A rough estimate is that this should be ≈ 10 orders of magnitude less intense than the allowed decay.

From the R-matrix fit to the total α spectrum a β^+ spectrum was deduced and compared to the data of Ref. [10]. Allowing the momentum calibration of Ref. [10] to be offset by a constant value, b , a minimum χ^2 of 31.8 was found for 33 data points and $b \approx 70 \pm 20$ keV/c. Thus this α spectrum predicts a harder β^+ spectrum than the calibrated spectrum of Ref. [10]. In this sense, this α spectrum is in rough agreement with the WA2 and DBW spectra.

Using the *distribution of strength* from the R-matrix fits to foils 1 and 2 the ${}^8\text{B}$ neutrino spectrum was de-

duced. Small radiative and forbidden corrections were included using the same formalism as in Ref. [1], except that more complete expressions were used for the forbidden corrections but the differences were found to be negligible. The best estimate of the ^8B ν spectrum was taken as the average of the spectra generated using the R-matrix parameters for foils 1 and 2 under condition A.

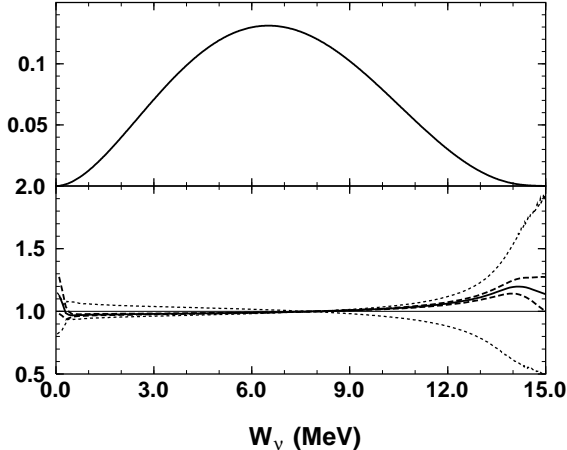


FIG. 4. Top panel: neutrino spectrum. Bottom panel: ratio between this neutrino spectrum and that of Ref. [1]. The dashed lines represent the uncertainties in this spectrum while the dotted lines represent the 3σ errors in Ref. [1].

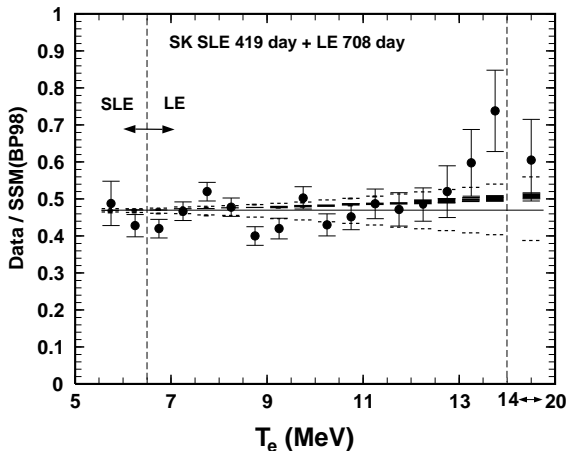


FIG. 5. The 708-day spectrum of electrons at SuperK divided by what is expected based on the ν spectrum shape of Ref. [1], and the solar model of Ref. [16] (BP98). The data points and total errors were taken graphically from Ref. [17]. Also plotted is 0.47 times [17] the ratio of the electron spectrum generated using this ν spectrum to that of Ref. [1] with the SuperK response function. The width of the solid line represents the uncertainty associated with this neutrino spectrum while the dotted lines represent the 3σ errors to the ν spectrum of Ref. [1].

The ratio of this ν spectrum to the best recommendation of Ref. [1] is shown in Fig. 4. Approximately 10 – 20% more neutrinos are found in the high-energy

end of the spectrum. The uncertainties in the ν spectrum were calculated in a similar way as explained above for the alpha spectrum except one more condition was added. The neutrino spectrum was generated using the data itself instead of an R-matrix fit. Figure 5 shows the implications of these findings with respect to the SuperKamiokande data. This spectrum implies a correction to Ref. [1]’s recommendation that ranges from $\approx 0\%$ at $T_e = 5$ MeV to $\approx 8\%$ at the endpoint.

The efficiencies of the ^{37}Cl , ^{71}Ga , ^{40}Ar , and SuperKamioka detectors are respectively, 3.6%, 1.4%, 5.7% and 1.8% larger than previously thought.

ACKNOWLEDGMENTS

We thank J.J. Kolata, F. Bechetti, D. Peterson, and P. Santi, for help during the early stages of this experiment, J. Napolitano for sending us the β^+ spectrum, and J.F. Beacom, R.G.H. Robertson and S.J. Freedman for illuminating comments. AG thanks the National Institute for Nuclear Theory at Seattle for hosting during the summer of 1999.

-
- [1] J.N. Bahcall, E. Lisi, D.E. Alburger, L. De Braeckeleer, S.J. Freedman and J. Napolitano, Phys. Rev. C **54**, 411 (1996).
 - [2] J.N. Bahcall, Phys. Rev. D **44**, 1644 (1991).
 - [3] R.G.H. Robertson, Presented at Lepton-Photon 99 Conference, Stanford, Aug. 9-14, 1999; to be published in the Proceedings; LANL hep-ex/0001034v2.
 - [4] J.N. Bahcall and P.I. Krastev, Phys. Lett. B **436**, 243 (1998).
 - [5] R. Schiavilla, Bull. Am. Phys. Soc. **44**, 28 (1999).
 - [6] F.L. Villante, Phys. Lett. B **460**, 437 (1999).
 - [7] J.N. Bahcall, P.I. Krastev, and A. Yu. Smirnov, Phys. Rev. D **60**, 093001 (1999)
 - [8] B.J. Farmer and C.M. Class, Nucl. Phys. **15**, 626 (1960).
 - [9] D.H. Wilkinson and D.E. Alburger, Phys. Rev. Lett. **26**, 1127 (1971).
 - [10] J. Napolitano and S.J. Freedman, Phys. Rev. C **36**, 298 (1987).
 - [11] S.K. Allison, Rev. Mod. Phys. **30**, 1137 (1958).
 - [12] Tables containing our alpha and deduced neutrino spectra can be found at www.nd.edu/~nsl/BeyondSM/boron8/tables.
 - [13] E.K. Warburton, Phys. Rev. C **33**, 303 (1986) and references therein.
 - [14] F.C. Barker, Aust. J. Phys. **42**, 25 (1989)
 - [15] DeBraeckeleer *et al.*, Phys. Rev. C **51**, 2778 (1995).
 - [16] J.N. Bahcall, S. Basu, and M. Pinsonneault, Physics Letters B **433**, 1 (1998).
 - [17] M.B. Smy, hep-ex/9903034